Inorg. Chem. **2009**, *48*, 1334−1338

Formation of CeO_2 Nanotubes from $Ce(OH)CO_3$ Nanorods through Kirkendall Diffusion

Guozhu Chen,[†] Sixiu Sun,*[,†] Xun Sun,[‡] Weiliu Fan,[†] and Ting You[†]

Key Laboratory of Colloid and Interface Chemistry, Ministry of Education, School of Chemistry and Chemical Engineering and State Key Laboratory of Crystal Materials, Shandong University, Jinan, 250100, People's Republic of China

Received June 24, 2008

In this paper, CeO_2 nanotubes based on the Kirkendall effect (for simplicity, this type of nanotubes is denoted as K-type CeO_2 nanotubes) are fabricated through a solid−liquid interface reaction between $Ce(OH)CO_3$ nanorods and NaOH solutions. Our studies indicate the formation mechanism of K-type CeO_2 nanotubes is quite different from those of CeO_2 nanotubes subjected to template (T-type CeO_2 nanotubes) and lamellar rolling (L-type CeO_2 nanotubes) reported previously by our group. The K-type CeO_2 nanotubes are prepared by congregating Kirkendall voids and subsequent calcinations. The time evolution processes are imaged by TEM, and the results show that as the reaction processes, interior spaces are formed and enlarged in $Ce(OH)CO_3$ nanorods to form K-type CeO_2 nanotubes. In contrast, the interior space in T-type CeO_2 nanotubes decreases with reaction time. XRD is applied to study the phase transformation in the formation process of K-type CeO_2 nanotubes. Our study also indicates NaOH and reaction temperature are two key factors responsible for formation of K-type CeO_2 nanotubes. Combined with the T- and L-type nanotubes, three types of CeO_2 nanotubes with different formation mechanisms are successfully synthesized in one reaction system, which might afford some guidance for the synthesis of other inorganic nanotubes.

Introduction

Nanotubes with hollow interiors have been extensively studied for their applications in many areas including catalysis, drug delivery, and protection of environmentally sensitive biological species.[1−4] Since the discovery of carbon nanotubes and WS_2 nanotubes in the 1990s, a wealth of inorganic nanotubes have been synthesized from corresponding layered compounds through rolling up of the 2D sheets under appropriate conditions.[5−10] Concerning the nanotubes from inorganic materials without a layered structure, several methods/phenomena, such as the Kirkendall effect, Ostwald ripening, and the template method, were successfully applied to fabricate them.[11−14] Among these methods, utilization of the Kikendall effect has been demonstrated and is a new alternative opportunity to direct nanotubes formation since the hollow CoO, Co_3S_4 nanoparticles were synthesized in 2004.[15] In a Kirkendall diffusion system, the difference in diffusion rates of two interdiffusion species across an interface results in a net directional flow of matter, which is balanced by an opposite flow of vacancies.[16−23] The hollow

* To whom correspondence should be addressed. Phone: 86-531-88365432. Fax: 86-531-88564464. E-mail: ssx@sdu.edu.cn.
† Key Laboratory of Colloid and Interface Chemistry.
‡ State Key Laboratory of Crystal Materials.

(1) Zhan, J.; Bando, Y.; Hu, J.; Yin, L.; Yuan, X.; Sekiguchi, T.; Golberg, D. *Angew. Chem., Int. Ed.* **2005**, *45*, 228.
(2) Zhou, W.; Han, Z.; Wang, J.; Zhang, Y.; Jin, Z.; Sun, X.; Zhang, Y.; Yan, C.; Li, Y. *Nano Lett* **2006**, *6*, 2987.
(3) Tan, Y.; Xue, X.; Peng, Q.; Zhao, T.; Wang, T.; Li, Y. *Nano Lett.* **2007**, *7*, 3723.
(4) Zhou, W.; Han, Z.; Wang, J.; Zhang, Y.; Jin, Z.; Sun, X.; Zhang, Y.; Yan, C.; Li, Y. *Nano Lett* **2006**, *6*, 2987.
(5) Iijima, S. *Nature* **1991**, *354*, 56.
(6) Tenne, R.; Margulis, L.; Genut, M.; Hodes, G. *Nature* **1992**, *360*, 444.
(7) Nath, M.; Rao, C. N. R. *J. Am. Chem. Soc.* **2001**, *123*, 4841.
(8) Li, Y. D.; Li, X. L.; He, R. R.; Zhu, J.; Deng, Z. X. *J. Am. Chem. Soc.* **2002**, *124*, 1411.
(9) Li, Y.; Wang, J.; Deng, Z.; Wu, Y.; Sun, X.; Yu, D.; Yang, P. *J. Am. Chem. Soc.* **2001**, *123*, 9904.
(10) Tang, C.; Bando, Y.; Huang, Y.; Yue, S.; Gu, C.; Xu, F.; Golberg, D. *J. Am. Chem. Soc.* **2005**, *127*, 6552.
(11) Liu, S. M.; Gan, L. M.; Liu, L. H.; Zhang, W. D.; Zeng, H. C. *Chem. Mater.* **2002**, *14*, 2427.
(12) Jia, C. J.; Sun, L. D.; Yan, Z. G.; You, L. P.; Luo, F.; Han, X. D.; Pang, Y. C.; Zhang, Z.; Yan, C. H. *Angew. Chem., Int. Ed.* **2005**, *44*, 4328.
(13) Xiong, Y.; Xie, Y.; Yang, J.; Zhang, R.; Wu, C.; Du, G. *J. Mater. Chem.* **2002**, *12*, 3712.
(14) Zhan, J.; Bando, Y.; Hu, J.; Golberg, D. *Inorg. Chem.* **2004**, *43*, 2462.
(15) Yin, Y.; Rioux, R. M.; Erdonmez, C. K.; Hughes, S.; Somorjai, G. A.; Alivisatos, A. P. *Science* **2004**, *304*, 711.
(16) Yan, C.; Xue, D. *Adv. Mater.* **2008**, *20*, 1055.

10.1021/ic801714z CCC: $40.75
Published on Web 01/15/2009

nanotubes were synthesized in a way that these vacancies coalesce into a single hollow core. For example, CuO nanotubes were synthesized by Zeng's group from direct metal oxidation based on the fact that copper moves preferentially toward the surface region while oxygen anions on the surface are relatively immobile.[24] Fan et al. successfully synthesized Ag_2Se nanotubes by UV photodissociation of adsorbed CSe_2 on the surface of Ag nanowires under ambient conditions where voids grew from both ends of the nanowires along the longitudinal axis and ultimately merged to form hollow nanotubes.[25]

Cerium oxide is one of the most reactive earth metal oxides, which has been extensively employed in various applications including oxygen storage capacitors, catalysts, UV blockers, and polishing materials.[26−28] As one of the inorganic materials that do not possess a layered structure, CeO_2 nanotubes require more effort to fabricate compared with layered compounds. For example, Tang et al. synthesized CeO_2 nanotubes by annealing $Ce(OH)_3$ nanotubes prepared under oxygen-free conditions.[29] Han et al. observed the coexistence of CeO_{2-x} nanowires, nanoparticles, and nanotubes by precipitation followed by a long period of aging (45 days) at 0 °C.[30] Synthesis of CeO_2 nanotubes with a large cavity and thin walls by an oxidation-coordination-assisted dissolution process of the $Ce(OH)_3$ nanotubes/nanorods was reported by Zhou.[31] All of these methods were either time consuming or required rigorous conditions. Moreover, only one type of nanotubes was obtained in each reaction system. Very recently, we reported two kinds of CeO_2 nanotubes with completely different morphologies and structures prepared in alkaline solutions by employing $Ce(OH)CO_3$ nanorods as precursors just slightly tuning the postprocessing conditions.[32] Formation of these two types of CeO_2 nanotubes involves employing either $Ce(OH)CO_3$ nanorods as both the physical and chemical templates (T-type) or the layered $Ce(OH)_3$ as an anisotropic intermediate species (L-type). In this paper, we found the third type of CeO_2 nanotubes (K-type) based on the Kirkendall effect, which still relies on the interface reaction between $Ce(OH)CO_3$ nanorods and NaOH aqueous solution. Owing to the similarity between K- and T-type nanotubes on their size, we analyzed systemically their difference and correlation. The $Ce(OH)CO_3$ precursor in the solid−liquid system is a crucial factor not only for T- and L-type nanotubes but also for K-type nanotubes formation. The K-type nanotubes structural details were provided by XRD, XPS, and TEM investigations.

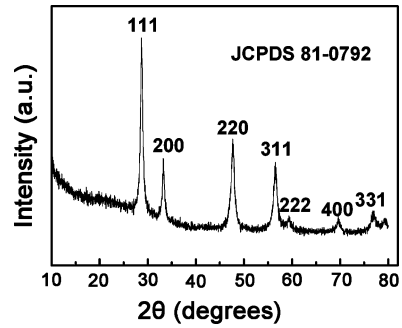

Figure 1. XRD pattern of K-type nanotubes.

Experimental Section

All reagents were of analytical grade and used without further purification. The synthetic routes and SEM/TEM images of $Ce(OH)CO_3$ precursor as well as T-, L-type nanotubes are shown in the Supporting Information. In a typical synthetic procedure of K-type CeO_2 nanotubes, the $Ce(OH)CO_3$ precursors (0.087 g) were dispersed into 20 mL of distilled water. Upon adding 0.96 g of NaOH the mixture solution was stirred for 30 min and then kept at room temperature. After 12 days, the light yellow precipitate was washed with distilled water and anhydrous alcohol several times and then dried at 60 °C for 12 h. The as-dried powder was calcined to produce yellowish ceria powder in air at 600 °C for 4 h.

The samples were characterized by X-ray diffraction (XRD) on a Japan Rigaku D/Max-γA rotating anode X-ray diffractometer equipped with graphite-monochromatized Cu Kα radiation (λ = 1.54178 Å) at a scanning rate of 0.02° s^{-1} in the 2θ range from 10° to 80°. The XRD pattern was analyzed by Rietveld refinement, which was carried out using the software Jade 5, as a means of establishing phase purity and sample quality. The morphology and structure of CeO_2 nanotubes were characterized by transmission electron microscopy (TEM, JEOL 6300, 100 kV) and high-resolution transmission electron microscopy (HRTEM, JEM-2100, 200 kV). XPS spectra were recorded on a ESCALAB 250 spectrometer with a standard Al Kα source. The charging of the samples was corrected by referencing all of the energies to the C 1s peak energy set at 285.1 eV, arising from adventitious carbon. The specific surface area of the products was determined from nitrogen absorption data obtained at low temperature (77 K) using an Qudrasorb SI instrument.

Results and Discussion

The phase and purity of the as-prepared products was examined by XRD (Figure 1). All of the reflections can be readily indexed to pure cubic fluorite CeO_2 with a lattice constant a = 5.148 Å (JCPDS Card No. 81-0792), and the broadening of the diffraction peaks indicates that the as-prepared samples were nanosized. As shown in Figure S1a, Supporting Information, good fits between the observed data and the profiles from JCPDS 81-0792 were obtained after a

(17) Yang, Y.; Kim, D. S.; Scholz, R.; Knez, M.; Lee, S. M.; Gosele, U.; Zacharias, M. *J. Phys. Chem. C* **2008**, *112*, 4068.
(18) Ng, C. H. B.; Fan, W. Y. *J. Phys. Chem. C* **2007**, *111*, 9166.
(19) Liang, X.; Wang, X.; Zhuang, Y.; Xu, B.; Kuang, S.; Li, Y. *J. Am. Chem. Soc.* **2008**, *130*, 2736.
(20) Chiang, R.-K.; Chiang, R.-T. *Inorg. Chem.* **2007**, *46*, 369.
(21) Tian, L.; Yang, X.; Lu, P.; Williams, I. D.; Wang, C.; Ou, S.; Liang, C.; Wu, M. *Inorg. Chem.* **2008**, *47*, 5522.
(22) Cao, H.; Qian, X.; Wang, C.; Ma, X.; Yin, J.; Zhu, Z. *J. Am. Chem. Soc.* **2005**, *127*, 16024.
(23) Ye, L.; Guo, W.; Yang, Y.; Du, Y.; Xie, Y. *Chem. Mater.* **2007**, *19*, 6331.
(24) Chang, Y.; Lye, M. L.; Zeng, H. C. *Langmuir* **2005**, *21*, 3746.
(25) Bernard Ng, C. H.; Tan, H.; Fan, W. Y. *Langmuir* **2006**, *22*, 9712.
(26) Shao, Z. P.; Haile, S. M.; Ahn, J. M.; Ronney, P. D.; Zhan, Z. L.; Barnett, S. A. *Nature* **2005**, *435*, 795.
(27) Deng, W.; Flytzani-Stephanopoulos, M. *Angew. Chem., Int. Ed.* **2006**, *45*, 2285.
(28) Kumar, P.; Sun, Y.; Idem, R. O. *Energy Fuels* **2007**, *21*, 3113.
(29) Tang, C.; Bando, Y.; Liu, B.; Golberg, D. *Adv. Mater.* **2005**, *17*, 3005.
(30) Han, W. Q.; Wu, L. J.; Zhu, Y. M. *J. Am. Chem. Soc.* **2005**, *127*, 12814.
(31) Zhou, K. B.; Yang, Z. Q.; Yang, S. *Chem. Mater.* **2007**, *19*, 1215.
(32) Chen, G.; Xu, C.; Song, X.; Zhao, W.; Ding, Y.; Sun, S. *Inorg. Chem.* **2008**, *47*, 723.

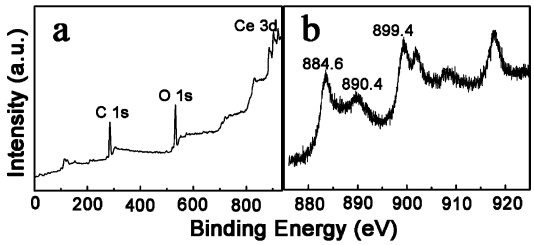

Figure 2. XPS patterns of K-type CeO_2 nanotubes: (a) survey spectra and (b) Ce 3d.

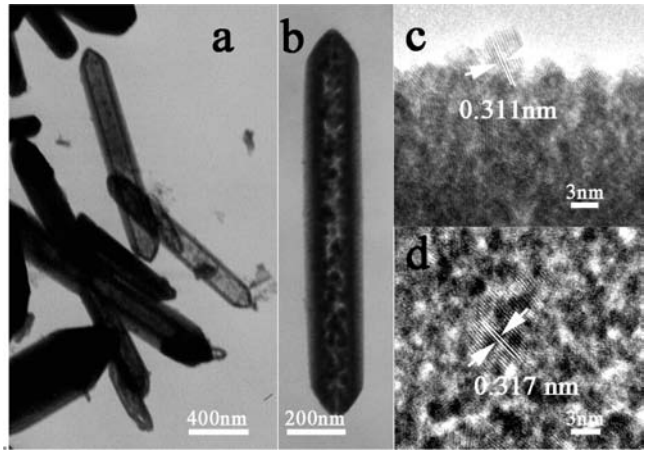

Figure 3. TEM image of the synthesized K-type CeO_2 nanotubes (a), high-magnification TEM image (b), and HR-TEM images from the shell (c) and interior space of the K-type nanotubes (d).

few cycles of refinement for all samples. No other crystalline impurities, such as $Ce(OH)CO_3$ precursor and $Ce(OH)_3$ intermediate, were detected by XRD, which show the high purity of the obtained K-type CeO_2 nanotubes (Figure S1b, Supporting Information). Figure 2 depicts the XPS spectra of the K-type nanotubes. Peaks of C 1s, O 1s, and Ce 3d can be identified from Figure 2a. In Figure 2b, we find six Ce 3d binding energy peaks of CeO_2 K-type nanotubes which are consistent with the previous report of Ce^{4+}. The peaks labeled 884.6 and 890.4 are attributed to Ce $3d^94f^2L^{n-2}$ and Ce $3d^94f^1L^{n-1}$ states; the peaks labeled 899.4 correspond to the Ce $3d^94f\ ^0L^n$ final state of Ce(IV) $3d_{5/2}$. Thus, it can be concluded that the main valence of cerium in the K-type nanotubes is +4.[33]

The morphologies of the precursors and resulting samples were investigated by transmission electron microscopy. As shown in Figure S2, Supporting Information, the rod-like $Ce(OH)CO_3$ precursors have a diameter of around 150−300 nm with lengths typically larger than 1 μm. Figure 3a shows the TEM image of converted CeO_2 nanostructures. One may observe that some particles hold a tubular structure verified by the brightness contrast between shell and core. The high-magnification TEM image in Figure 3b exhibits the detailed structure of K-type CeO_2 nanotubes. It is interesting that the interior space of K-type nanotubes is not fully vacant but with segmented voids, which is distinct from that of T-type nanotubes with thorough hollowing. Figure 3c and 3d show the lattice-resolved HRTEM images of the shell and interior space. The clear lattice image indicates the high crystallinity of the K-type nanotubes. The lattice spacing of 0.317 and 0.311 nm calculated from the HRTEM images for the (111) planes is typical of the cubic CeO_2 structures. The results of BET measurements showed that the specific surface area of K-type nanotubes was 50.02 m^2/g. The high surface area of the nanotubes may be attributed to their tiny crystal size and hollow structure.

To understand the mechanism of this kind of nanotubes, the growth process of CeO_2 nanotubes was investigated in detail at different reaction times. As depicted in Figure 4a, when the interface reaction proceeded for 6 days, the K-type nanotubes has hardly brightness contrast between the shell and the core in the TEM images. When the interface reaction time is prolonged to 9 days, the segmented voids appear in the K-type nanotubes. The tendency that the pore enlarges at the center becomes more obvious after 12 days of the interface reaction. On the basis of the experimental results, it can be concluded that there might exist another formation mechanism different from those of CeO_2 nanotubes subjected to template (T-type) and lamellar rolling (L-type) we reported before. In fact, there is also a liquid−solid interface reaction between the OH^- and $Ce(OH)CO_3$ precursors. Herein, the $Ce(OH)CO_3$ precursor acts as both site template and reactant. Using $Ce(OH)CO_3$ nanorods as templates, we anticipate receiving CeO_2 hollow nanostructures of similar morphology according to the reaction given below

$$Ce(OH)CO_3 \rightarrow Ce^{3+} + OH^- + CO_3^{2-} \quad (1)$$

$$Ce^{3+} + 3OH^- \rightarrow Ce(OH)_3 \quad (2)$$

$$Ce(OH)_3 \xrightarrow{O_2} Ce(OH)_4 \quad (3)$$

$$Ce(OH)_4 \xrightarrow{\text{calcination}} CeO_2 \quad (4)$$

When an appropriate amount of $Ce(OH)CO_3$ is introduced into the NaOH aqueous solution, $Ce(OH)CO_3$ nanorods dissociate slowly to produce Ce^{3+}, OH^-, and CO_3^{2-} ions in solution (eq 1). The coupled reaction/diffusion (eq 2) at the solid−liquid interface leads to quick formation of an interconnected $Ce(OH)_3$ shell around the external surface of the $Ce(OH)CO_3$ nanorods. The outer $Ce(OH)_3$ shell prevents a direct chemical reaction, and further reaction relies on diffusion of Ce^{3+} and OH^- through the shell. It is noted that due to the different ionic radii between Ce^{3+} and OH^-, the outward diffusion of Ce^{3+} in the $Ce(OH)CO_3$ core is faster than inward diffusion of OH^- ions in solution, a net outflow of Ce^{3+} ions through the $Ce(OH)_3$ shell results in the opposite transport of lattice vacancies. Thus, small interior space is obtained based on a nonequilibrium interdiffusion process and schematically displayed in Figure 4c. Owing to the Ce(III) oxidation state being unstable as compared with the Ce(IV) oxidation state in alkaline solution and in the presence of air, Ce^{3+}/Ce^{4+} oxidation is favored at higher pH and conversion from $Ce(OH)_3$ to $Ce(OH)_4$ ($CeO_2 \cdot 2H_2O$) can be realized easily (eq 3). As for formation of CeO_2, not only can $Ce(OH)_4$ be dehydrated but

(33) Zhong, L. S.; Hu, J. S.; Cao, A. M.; Liu, Q.; Song, W. G.; Wan, L. J. *Chem. Mater.* **2007**, *19*, 1648.
(34) Fan, H. J.; Gosele, U.; Zacharias, M. *Small* **2007**, *3*, 1660.

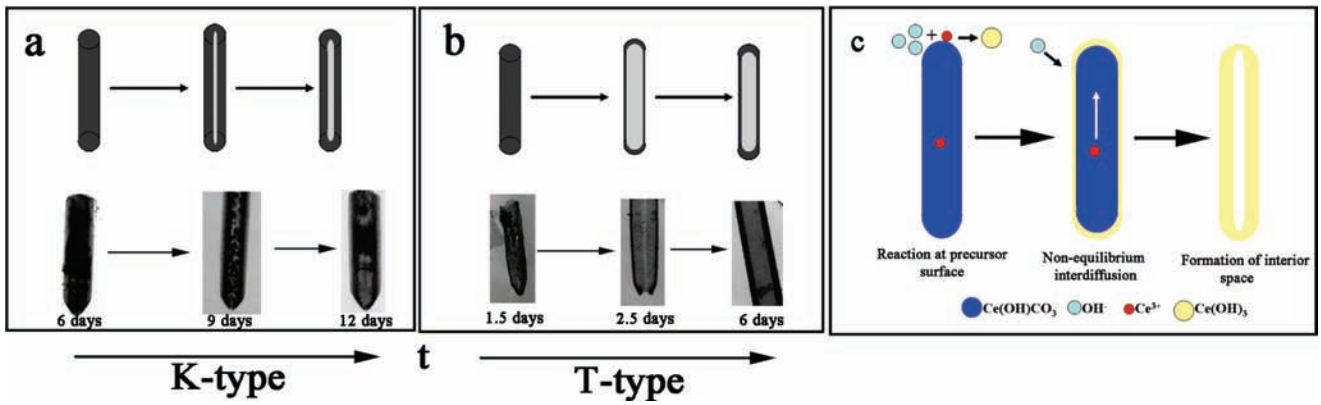

Figure 4. Sketch map and corresponding TEM images of evolution processes for K-type (a) and T-type (b) nanotubes; (c) schematic illustration of the procedure used to fabricate K-type nanotubes.

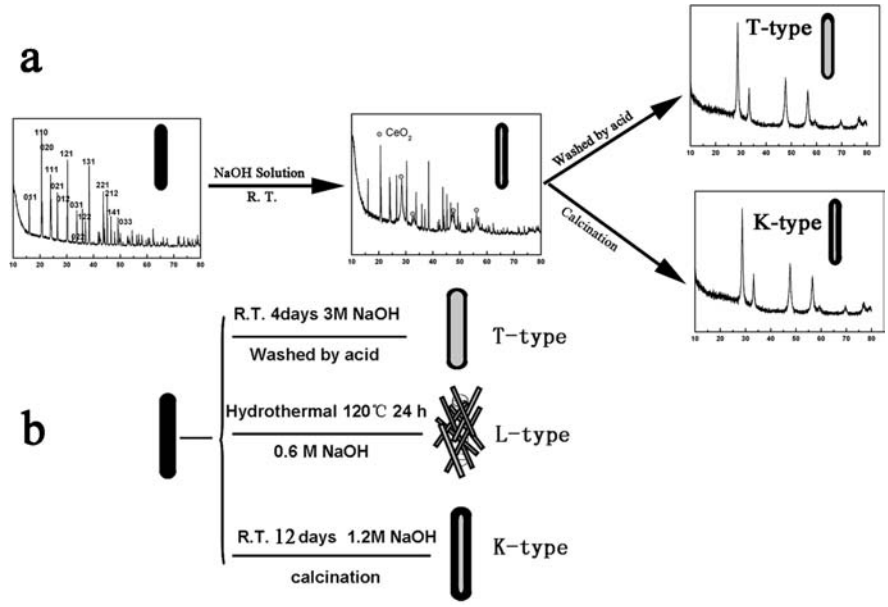

Figure 5. (a) Sketch map and corresponding XRD patterns depicting the correlation between the T- and K-type CeO_2 nanotubes. (b) Formation processes of three different CeO_2 nanotubes.

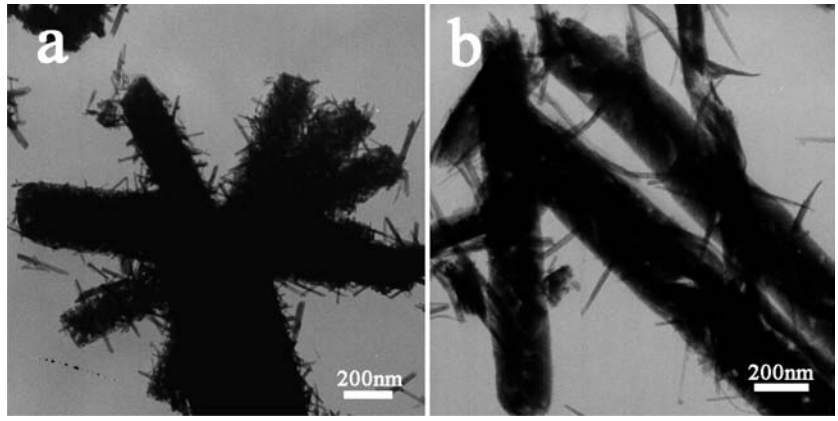

Figure 6. TEM images of typical particles synthesized under different conditions: (a) 1.2 M NaOH, 120 °C for 2 days and (b) 9 M NaOH, room temperature for 6 days.

also unreacted $Ce(OH)CO_3$ can be decomposed completely during a later calcination process in air (eq 4). As shown in Figure 3b, discontiguous voids are roughly located at the center, which can be explained by preferential enlargement of some early established voids by losing surface atoms and the net inward flow of vacancies converged in a bigger space.[30] All of these indicate this type of nanotubes are formed by Kirkendall diffusion. Although the yield of K-type nanotubes is low (<10%), it still gives illumination to realize the formation mechanisms of nanotubes. Work in searching for the optimal condition to acquire high-yield nanotubes is currently in progress.

To further demonstrate the formation mechanism based on the Kirkendall diffusion, we compare K-type nanotubes with T-type nanotubes owing to the similarity of their sizes and morphologies (because L-type nanotubes with a smaller size are obtained not at room temperature but under the hydrothermal condition, here we no longer compare it with K-type nanotubes). For T-type nanotubes, the $Ce(OH)_3$ shell formed at the early stages can be converted into CeO_2 by aging with concentrated NaOH. Subsequently, the unreacted $Ce(OH)CO_3$ nanorod cores washed away by diluted HNO_3 result in a large interior space in the T-type nanotubes. Therefore, the thicker shell and enlargement of interior space is acquired in the T-type nanotubes as the interface reaction proceeds. Figure 4b shows the time-dependent evolution TEM images of T-type nanotubes. When the interface reaction has proceeded for 1.5 days, T-type nanotubes with a very thin shell and large interior space were observed. When the interface reaction time was prolonged to 2.5 days, the thickness of the shell becomes thicker and the interior space shrinks slightly. The tendency becomes more obvious when the reaction time was increased to 6 days. The obvious, opposite variational tendency as the interface reaction time shown in Figure 4 discloses the K- and T-type nanotubes are subjected to different formation mechanisms. In fact, the Kirkendall diffusion happens equally in the formation process of T-type nanotubes. In other words, the discontiguous voids have come into being already before washing by acid in the process of T-type nanotubes formation. Once washed by acid, the voids aroused by the Kirkendall diffusion and voids produced by dissolving the unreacted $Ce(OH)CO_3$ merge, which result in an enlarged interior space in T-type nanotubes. The small interior space resulting from Kirkendall diffusion retains its size after calcinations in K-type nanotubes. This is the reason why the TEM images brightness contrast between core and shell is obvious in the T-type nanotubes, while it is unconspicuous in the K-type nanotubes. The correlation between the T-type and the K-type nanotubes is depicted in Figure 5a. From the structural evolution confirmed by XRD analysis, one sees the coexistence of $Ce(OH)CO_3$ and CeO_2 before posttreatment. High purities of CeO_2 nanotubes are all obtained after acid washing for T-type and calcinations for K-type.

Suitable reaction temperature and reactant concentration are important and should ensure sufficient diffusivities of the atoms and vacancies. Figure 6 show the effects of temperature and concentration. Because the solid−liquid interface reaction initiates and proceeds preferentially on the surface of $Ce(OH)CO_3$ nanorods, one sees that the final 1D CeO_2 exhibits a bundle-like structure in a controlled fashion, where the original template shape can still be distinguished when the reaction temperature is increased to 120 °C. The concentration of NaOH solution also influences formation of hollow structures. Generally speaking, high temperature and concentration favor diffusion, and it seems that it facilitates formation of K-type nanotubes in our experiments. Unfortunately, the experimental results show that the higher the NaOH solution concentration and/or the reaction temperature, the easier the formation of CeO_2 nanorods rather than nanotubes, as shown in Figure 6a and 6b. These results indicate that the dissolution/recrystallization rate drives the anisotropic growth of the hexagonal $Ce(OH)_3$ crystal nuclei, which is consistent with previous reports.[32,35]

Although oxidation decomposition of $Ce(OH)CO_3$ at high temperature has been applied to prepare CeO_2 nanoparticles, to the best of our knowledge, there is no report on the preparation of CeO_2 nanoparticles in solution using $Ce(OH)CO_3$ as a precursor.[35,36] The interesting point of using $Ce(OH)CO_3$ nanorods relies on its slow kinetics of a solid−liquid interface reaction between hard-soluble $Ce(OH)CO_3$ nanorods and NaOH aqueous solution. Experimental results showed that $Ce(OH)CO_3$ is responsible for the three types of nanotubes formation in NaOH solution. First, unreacted $Ce(OH)CO_3$ precursor is easily removed by inorganic acid and gives the opportunity for T-type CeO_2 nanotubes' formation. Second, $Ce(OH)_3$ possessed a layered structure, the product of reaction between NaOH and $Ce(OH)CO_3$, converts into L-type CeO_2 nanotubes through the lamellar rolling of $Ce(OH)_3$ nanosheets and subsequent oxidation. Third, different diffusivities of ions in the diffusion couple (Ce^{3+} and OH^-) would give the necessary conditions for the Kirkendall effect diffusion in the solid−liquid interface reaction, so the K-type nanotubes form. Finally, the $Ce(OH)CO_3$ precursor can be converted into CeO_2 at elevated temperature, which assures the purity of the K-type CeO_2 nanotubes. Formation processes of three different CeO_2 nanotubes are shown in Figure 5b.

Conclusions

We synthesized CeO_2 nanotubes based on the Kirkendall diffusion. Different formation mechanisms lead to the opposite variational tendency of void spaces between K-type and T-type nanotubes, although the formation process of T-type nanotubes accompanies Kirkendall diffusion. Owing to the high chemical potential for driving the anisotropic growth of the $Ce(OH)_3$ nuclei, high temperature and/or high NaOH concentration favor formation of 1D nanowires/nanorods instead of K-type nanotubes. The $Ce(OH)CO_3$ precursors play an important role for the three types of nanotubes formation. More importantly, it elucidates that different nanotubes subjected to different formation mechanisms in the same system can probably be applied in other metal oxides by rationally choosing suitable precursors.

Acknowledgment. This work was supported by the National 973 (2005CB623601) Program Projects of China.

Supporting Information Available: Rietveld refined powder XRD data for as-prepared K-type CeO_2 nanotubes; synthetic routes and SEM/TEM images of $Ce(OH)CO_3$ precursor, T- and L-type nanotubes. This material is available free of charge via the Internet at http://pubs.acs.org.

IC801714Z

(35) Guo, Z. Y.; Du, F. L.; Li, G. C.; Cui, Z. L. *Inorg. Chem.* **2006**, *45*, 4167.
(36) Qi, R. J.; Zhu, Y. J.; Cheng, G. F.; Huang, Y. H. *Nanotechnology* **2005**, 2502.